Evolutionary rate covariation analysis of E-cadherin identifies Raskol as regulator of cell adhesion and actin dynamics in *Drosophila*

Short title: Raskol regulates border cell migration in the *Drosophila* egg chamber

Qanber Raza[1], Jae Young Choi[2], Yang Li[1], Roisin M. O'Dowd[1], Simon C. Watkins[1,3], Yang Hong[1], Nathan L. Clark[4], Adam V. Kwiatkowski[1*]

[1] Department of Cell Biology, University of Pittsburgh School of Medicine, Pittsburgh, PA, USA

[2] Center for Genomics and Systems Biology, Department of Biology, New York University, New York, NY USA

[3] Center for Biologic Imaging, University of Pittsburgh School of Medicine, Pittsburgh, PA, USA

[4] Department of Computational and Systems Biology, University of Pittsburgh, Pittsburgh, PA, USA

* Corresponding author

E-mail: adamkwi@pitt.edu (AVK)

Abstract

The adherens junction couples the actin cytoskeletons of neighboring cells to provide the foundation for multicellular organization. The core of the adherens junction is the cadherin-catenin complex that arose early in the evolution of multicellularity to link cortical actin to intercellular adhesions. Over time, evolutionary pressures have shaped the signaling and mechanical functions of the adherens junction to meet specific developmental and physiological demands. Evolutionary rate covariation (ERC) identifies genes with correlated fluctuations in evolutionary rate that can reflect shared selective pressures and functions. Here we use ERC to identify genes with evolutionary histories similar to *shotgun (shg)*, which encodes the *Drosophila* E-cadherin (DE-Cad) ortholog. Core adherens junction components α-catenin and p120-catenin displayed strong ERC correlations with *shg*, indicating that they evolved under similar selective pressures during evolution between *Drosophila* species. Further analysis of the *shg* ERC profile revealed a collection of genes not previously associated with *shg* function or cadherin-mediated adhesion. We then analyzed the function of a subset of ERC-identified candidate genes by RNAi during border cell (BC) migration and identified novel genes that function to regulate DE-Cad. Among these, we found that the gene *CG42684*, which encodes a putative GTPase activating protein (GAP), regulates BC migration and adhesion. We named *CG42684 raskol* (“to split” in Russian) and show that it regulates DE-Cad levels and actin protrusions in BCs. We propose that Raskol functions with DE-Cad to restrict Ras/Rho signaling and help guide BC migration. Our results demonstrate that a coordinated selective pressure has shaped the adherens junction and this can be leveraged to identify novel components of the complexes and signaling pathways that regulate cadherin-mediated adhesion.

41 ## Author Summary

42 The establishment of intercellular adhesions facilitated the genesis of
43 multicellular organisms. The adherens junction, which links the actin cytoskeletons of
44 neighboring cells, arose early in the evolution of multicellularity and selective pressures
45 have shaped its function and molecular composition over time. In this study, we used
46 evolutionary rate covariation (ERC) analysis to examine the evolutionary history of the
47 adherens junction and to identify genes that coevolved with the adherens junction gene
48 *shotgun*, which encodes the *Drosophila* E-cadherin (DE-Cad). ERC analysis of *shotgun*
49 revealed a collection of genes with similar evolutionary histories. We then tested the
50 role of these genes in border cell migration in the fly egg chamber, a process that
51 requires the coordinated regulation of cell-cell adhesion and cell motility. Among these,
52 we found that a previously uncharacterized gene *CG42684*, which encodes a putative
53 GTPase activating protein (GAP), regulates the collective cell migration of border cells,
54 stabilizes cell-cell adhesions and regulates the actin dynamics. Our results demonstrate
55 that components of the adherens junction share an evolutionary history and that ERC
56 analysis is a powerful method to identify novel components of cell adhesion complexes
57 in *Drosophila*.

58

Introduction

The adherens junction (AJ) is a multiprotein complex that is essential for intercellular adhesion in metazoa. The core of the AJ is the cadherin-catenin complex. Classical cadherins are single-pass transmembrane proteins with an extracellular domain that mediates calcium-dependent homotypic interactions. The adhesive properties of classical cadherins are driven by the recruitment of cytosolic catenin proteins to the cadherin tail: p120-catenin binds to the juxta-membrane domain and β-catenin binds to the distal part of the tail. β-Catenin recruits α-catenin to the cadherin-catenin complex. α-Catenin is an actin-binding protein and the primary link between the AJ and the actin cytoskeleton [1-3].

The primary function of the AJ is to link actin to intercellular junctions. It is believed the AJ arose early in the evolution of multicellular metazoans to coordinate epithelial tissue formation and organization [4-7]. The AJ has since evolved to function in a range of physiological and developmental processes, including cell polarity, collective cell migration and cell division [8, 9]. AJ function in these diverse processes requires an array of ancillary regulatory proteins, including kinases, signaling molecules and adaptor proteins [10-14]. Defining the molecular networks that regulate AJ biology is critical to understanding cadherin-mediated adhesion in normal and disease states.

Evolutionary rate covariation (ERC) analysis is a comparative genomic approach that has been used successfully to identify genes with shared functions in canonical protein complexes and biological processes in prokaryotes, fungi, *Drosophila* and mammals [15-21]. ERC analysis takes advantage of the evolutionary rates shared between co-functional genes that have correlated rates of change due to common

selective pressures. ERC represents the correlation coefficient of branch-specific evolutionary rates that are estimated from the phylogenetic trees of a pair of genes and their orthologs from multiple species[19]. ERC analysis permits the identification of genes within a given genome that evolved in a correlated manner and hence might function in the same pathway or molecular complex. These genes can then be screened by RNAi-based knockdown or similar genetic approaches to validate their role in a relevant biological process.

Border cell (BC) migration in the developing *Drosophila* egg chamber requires coordinated cell adhesion and migration. During BC migration, a group of 6-8 follicular cells delaminate from the anterior most tip of the epithelium and undergo haptotaxis and migrate collectively towards the developing oocyte [22, 23]. The BC cluster consists of migratory BCs and a centrally positioned pair of polar cells (PCs) that signal to BCs and contribute to cluster adherence [23]. BC migration is highly dependent on *Drosophila* E-Cadherin (DE-Cad, encoded by *shotgun* (*shg*)) [24-26]. Upregulation of DE-Cad is essential for the initial delamination and subsequent migration of BC since disruption of DE-Cad-mediated adhesion affects the ability of BC to detach from the follicular epithelium (FE) and collectively migrate [24, 25].

We performed ERC analysis of *shg* to identify genes that share a common evolutionary history, and therefore may share an overlapping function, with *shg* and assessed their role in BC migration. Genes encoding the primary components of AJ, including *α-Cat* and *p120-catenin*, display high ERC values relative to *shg* and one another, suggesting that these genes and their protein products are co-functional, which is well described in the literature [1, 27]. We show that genes showing high ERC values

105 with *shg* are enriched for membrane-associated proteins and proteins that function in E-
106 cadherin-dependent biological processes. We then conducted an RNAi-mediated
107 genetic screen in BCs with 34 high-ranking ERC candidates and identified both novel
108 and known genes that function to regulate DE-Cad at cell contacts. Among those, we
109 characterized a GTPase activating protein (GAP) domain encoding gene, *CG42684*,
110 which we have named "*raskol*" after the Russian term "to split". We show that Raskol
111 colocalizes with DE-Cad, regulates DE-Cad levels at the BC-BC interface and
112 modulates actin-rich protrusions during BC migration. Our results demonstrate that
113 components of the AJ share an evolutionary history and that ERC analysis is a powerful
114 method to identify novel components of cell adhesion complexes in *Drosophila*.

115 ## Results

116 ### ERC analysis identifies genes that coevolved with *shg*

117 We used ERC analysis to identify novel genes that regulate DE-Cad-mediated
118 adhesion in *Drosophila*. Since ERC signatures are often observed between proteins that
119 function in a molecular complex [15, 16, 18, 19], we evaluated the ERC values of the fly
120 AJ components – *shotgun* (*shg*, DE-Cad), *armadillo* (*arm*; β-catenin in vertebrates), *α-*
121 *catenin* (*α-Cat*), *p120-catenin* (*p120ctn*), *Vinculin* (*Vinc*) and *canoe* (*cno*, afadin in
122 vertebrates). Notably, *shg*, *α-Cat* and *p120ctn* displayed positive ERC values with each
123 other (Fig 1A). *arm*, *Vinc* and *cno* did not show elevated ERC values relative to *shg*, α-
124 *Cat* or *p120ctn*. Since Arm, Vinc and Cno are known to function independently of
125 cadherin-mediated adhesion [28-31], we speculate that alternative selective pressures
126 have influenced the evolution of these genes in flies, likely obscuring any ERC signature
127 with purely AJ genes. Nonetheless, ERC analysis suggested that the AJ components

Genes	ERC value	Function in flies	Ortholog(s) (score*)	Ortholog function in mammals
grk	0.62	Growth factor (EGF)	Nrg (1/15)	EGF family receptor ligand
cac	0.62	Voltage-gated Ca^{2+} channel subunit	Cacna1 (11/15)	Voltage-gated Ca^{2+} channel subunit

DE-Cad, α-Cat and p120ctn coevolved to maintain their collective function in cell-cell adhesion. We postulated that other genes whose products regulate AJ biology would have similar evolutionary histories to maintain functionality.

We then used ERC analysis to identify genes with high ERC values relative to the core of the AJ complex, *shg* (S1 Table). We identified 137 genes with ERC values of 0.4 or greater, representing the top 1.3% of *shg* ERC values. Since α-*Cat* has an ERC value of 0.47 relative to *shg* (Fig 1A), placing their ERC value in the top 0.6 % of all gene pairs, we reasoned that genes with similar or higher ERC values would represent genes with similar evolutionary histories to *shg*. Accordingly, the thresholded *shg* ERC list contains genes with described roles in AJ regulation such as *Hrb98DE* [32, 33], *PDZ-GEF* [34, 35], *babo* [36, 37], *CG16952* [38, 39] and *Rab5* [40-42] (Table 1). Excitingly, the majority of identified genes have not been associated with the AJ and include transcription factors, kinases, GTPase regulatory proteins and calcium channel regulators (Table 1). A previous genomic RNAi screen conducted in *Drosophila* S2 cells [43] and E-Cadherin proximity biotinylation screens in epithelial cells [44, 45] identified multiple hubs of interactors and regulators. Cross referencing the *shg* ERC list with the hits from these screens revealed only a few common genes such as *RhoGAPp190*, *Rab5*, *Appl* and *Stim*. This suggests that ERC analysis is identifying additional *shg* regulatory components that were undetected in genetic or proteomic screens.

Hrb98DE	0.54	mRNA binding	Hnrnpa2b1 (13/15)	RNA binding protein
PDZ-GEF	0.53	Rap1 GEF	Rapgef2 (13/15)	Rap GEF
			Rapgef6 (12/15)	
Rab5	0.52	Rab GTPase; protein trafficking	Rab5c (13/15)	Rab GTPase; protein trafficking
			Rab5b (14/15)	
Stim	0.52	Ca^{2+} channel regulator	Stim1 (13/15)	Ca^{2+} influx regulation
raskol CG42684	0.50	GTPase activator activity (inferred)	Dab2ip (8/15)	Ras-GAP
			Rasal2 (8/15)	Ras-GAP
			Syngap1 (7/15)	Synaptic Ras-GAP
babo	0.5	Activin (TGFβ) receptor	Tgfbr1 (14/15)	TGF-β receptor
			Acvr1 (11/15)	
Gug	0.49	Nuclear repressor	Rere (10/15)	Transcriptional repressor
Pdk1	0.46	Kinase; cell signaling	Pdpk1 (11/15)	Kinase; cell signaling
CG16952	0.46	-	Btbd7 (10/15)	Branching morphogenesis
CG11593	0.46	-	Bnip2 (6/15)	Rho GTPase signaling
CG14883	0.44	-	Gde1 (12/15)	Glycerophosphodiester phosphodiesterase

Using gene ontology (GO) based enrichment analysis, we found that the *shg* ERC genes are enriched for plasma membrane (PM) localized proteins and PM-associated protein complexes (Fig 1B). Additionally, genes that function in biological processes requiring E-cadherin-mediated adhesion, such as wing disc morphogenesis, imaginal disc morphogenesis, epithelial morphogenesis, cell migration and AJ organization, were significantly overrepresented in the *shg* ERC list (Fig 1C). Next, we

Table 1. Function of selected conserved genes identified in *shg* ERC analysis. *Score from flybase (www.flybase.org) orthologue database. Ratio indicates sequence alignment algorithms that reported significant homology with mammalian orthologues.

154 analyzed the molecular functions of the human orthologs of the ERC identified genes.
155 We found that genes involved in epithelial AJ remodeling and cancer molecular
156 mechanism were overrepresented (Fig 1D; S2 and S3 Table). Also, genes that function
157 in RhoA, CCR5, TGF-β, PTEN and AJ-mediated signalling pathways were enriched (Fig
158 1D, S2 and S3 Table). Thus, the *shg* ERC list contains genes with established roles in
159 regulating AJs as well as novel candidate genes.

160 **RNAi screen in BCs identifies genes that regulate cell-cell adhesion**

161 To evaluate the function of genes in the *shg* ERC list, we conducted an *in vivo*
162 RNAi-based genetic screen in the *Drosophila* egg chamber. We analyzed BC collective
163 cell migration (CCM) because it is regulated by DE-Cad and is a powerful system to
164 study the interplay between cell migration and cell-cell adhesion (Fig 2A) [23, 24]. BC
165 detachment from the FE and concomitant CCM requires increased DE-Cad expression
166 and loss of DE-Cad arrests BC migration [24, 25].

167 First, we downregulated levels of individual AJ genes by using the GAL4/UAS
168 system to drive UAS-RNAi transgenes in the migrating BC cluster. We used a BC
169 specific driver, *slowborder*-GAL4 (*slbo*-GAL4) [46, 47] to drive expression of a UAS-
170 GFP reporter and a UAS-RNAi transgene targeted against the gene of interest. Stage
171 10 egg chambers expressing RNAi and GFP in BCs were fixed and scored for BC
172 cluster position along the anterior-posterior migration axis (Fig 2H). In control egg
173 chambers, nearly all BC clusters completed migration and were positioned adjacent to
174 the oocyte (Fig 2B and 2I). In contrast, downregulation of *shg* caused a BC migration
175 failure or delay in all egg chambers (Fig 2C and 2I). BC migratory defects were less
176 severe in egg chambers with reduced expression of *α-Cat* compared to *shg*; however,

177 the prevalence of defects was higher than in control egg chambers (Fig 2I). We could
178 not assess the effect of *arm* downregulation since *arm* RNAi expressing flies did not
179 survive to adulthood. The downregulation of *CadN, Vinc, p120ctn* or *cno* did not lead to
180 BC migratory defects (Fig 2I).

181 Next, we screened 34 genes from the *shg* ERC list. We focused on genes that
182 are expressed in the ovary [48] and for which an RNAi stock was readily available (S4
183 Table). The downregulation of target genes displayed a variable range of BC migration
184 defects with 12 genes displaying defects in more than 15% of egg chambers assessed
185 compared to 4% in control (Fig 2J). We also randomly selected and screened six genes
186 that had either very low ERC values or did not appear in the *shg* ERC list for migration
187 defects. As expected, we did not observe strong migration defects when these genes
188 were knocked down (Fig 2K). Moreover, the *shg* ERC genes showed statistically lower
189 average migration than the random negative control genes (Wilcoxon rank sum test,
190 p=0.0162), supporting the hypothesis that genes with correlated evolutionary histories
191 share functional characteristics. *Pdk1* knockdown resulted in the most penetrant
192 phenotype with 50% of egg chambers displaying either a failure or delay in BC
193 migration (Fig 2D and 2J). Knockdown of *babo* and *CG42684* caused migration delays
194 similar to *α-Cat* (Fig 2E–J). Additionally, knockdown of multiple genes resulted in
195 considerable migration delays relative to the control including *CG16952* (Fig 2D),
196 *Hrb98DE*, *magu*, *InR*, *RhoGAPp190*, *PDZ-GEF* and *CG11593* (Fig 2J). Conversely,
197 knockdown of genes such as *enc*, *mppe* and *rfx* did not affect BC migration (Fig 2J).

198 While screening *α-Cat* knockdown egg chambers, we noticed that about 20% of
199 the egg chambers displayed a cluster disassociation phenotype where one or more BCs

had separated from the cluster (Fig 3B and 3G). Since this phenotype is indicative of cell adhesion defects in BCs [24], we scored cluster disassociation for all genotypes. In control BCs expressing luciferase RNAi, disassociated clusters were rarely observed (Fig 3A and 3G). Likewise, downregulation of genes with low ERC values did not show a cluster disassociation phenotype (Fig 3I). Knockdown of *CadN*, *vinc*, *p120ctn* and *cno* also did not cause a penetrant cluster disassociation phenotype (Fig 3G). However, cluster disassociation phenotypes were observed with a number of ERC target genes. *CG42684, PDZ-GEF, CG16952, CG11593, zormin, cac* and *Rab5* displayed similar or higher cluster disassociation phenotypes compared to *α-Cat* (Fig 3). Overall, these ERC target genes, chosen for their high *shg* ERC values, exhibited the cluster disassociation phenotype significantly more often than genes with low *shg* ERC values (Wilcoxon rank sum test, p= 0.00022). Together, these results demonstrate that highly ranked genes in the *shg* ERC list contain factors that may regulate cell adhesion during BC collective cell migration.

Top ERC candidates regulate DE-Cad levels in BCs

Since knockdown of a subset of *shg* ERC list genes disrupted BC migration, we hypothesized that these genes might regulate DE-Cad at BC contacts. To test this, we quantified DE-Cad levels along cell-cell contacts between BCs in RNAi-expressing clusters. We used a DE-Cad-GFP knock-in stock that express DE-Cad at endogenous levels [49] and drove RNAi constructs under the control of *slbo*-GAL4. In control egg chambers where either luciferase RNAi or RFP were expressed, high DE-Cad levels were observed at BC-BC contacts (Fig 4A, S2A Fig). As expected, *shg* RNAi expression severely reduced DE-Cad levels in the BC cluster (Fig 4B). Knockdown of *CG42684*

(Fig 4C), *CG16952* (Fig 4D), *CG11593* (Fig 4E), *babo* (Fig 4G) and *Hrb98DE* (S2B Fig) caused a significant reduction in DE-Cad levels at BC-BC contacts. Interestingly, knockdown of *Pdk1*, a kinase in the PI3K pathway [50], did not affect DE-Cad levels in BCs even though it displayed the most prominent migration defect (Fig 4F). As expected, expression of RNAi for genes *capt* and *CG5872*, which have very low ERC values relative to *shg* and were therefore not predicted to operate in this pathway, did not cause a reduction in DE-Cad levels at BC-BC contacts (S2C and S2D Fig). Collectively, these results indicate that a significant subset of genes with high ERC values relative to *shg*, many of which were previously not associated with cadherin function, regulate DE-Cad levels at BC-BC contacts.

Raskol colocalizes with DE-Cadherin

Knockdown of *CG42684* displayed the most severe cell disassociation phenotype amongst all genes tested (Fig 3). CG42684 is reported to localize at the cell cortex and is enriched specifically at the apical surface of epithelial cells in *Drosophila* embryo [51] though almost nothing is known about its molecular function in flies. The mammalian orthologs of CG42684, Rasal2 and Dab2IP, also localize to the PM [52]. Interestingly, and similar to the impact we report here for CG42684, downregulation of Rasal2 disrupts E-Cadherin localization at the cell contacts [53], though the mechanism for this disruption remains poorly defined and its conservation across phyla has yet to be reported. Therefore, we wanted to determine whether CG42684, which we named "Raskol" (Russian for "to split") associates with DE-Cad along the cell membrane. Consistent with earlier localization studies, a YFP-trap stock expressing Raskol-YFP localized to the cell periphery in embryonic epidermal cells (S3 Fig) [51]. We used this

stock to assess Raskol colocalization with DE-Cad along the BC membrane. In *Drosophila* stage 8 embryos, before BCs have delaminated, Raskol localized to the cell membrane of BCs and PCs and was enriched at the PC apical membrane (Fig 5A, S2B Fig). During migratory stages, Raskol localization persisted at the PC apical membrane and at the cell-cell contacts of BCs and PCs (Fig 5B). Immunolabeling of egg chambers with DE-Cad antibody or imaging of endogenously RFP-tagged DE-Cad revealed strong colocalization between DE-Cad and Raskol (R=0.63, n=15) at the apical surface of PCs and at BC-BC contacts (Fig 5C and 5D). We also observed colocalization in the FE, particularly along the apical membrane (Fig 5A and 5C; S2A and S2B Fig). Raskol was not present at cell contacts between NCs (S2B Fig).

Next, we determined whether Raskol colocalizes with DE-Cad in other tissues that require AJ-mediated adhesion. Dorsal closure (DC) is an embryonic process in which the migrating ectoderm closes the dorsal hole [54-56]. The amnioserosa, an extra-embryonic tissue, covers the dorsal hole and contributes to ectodermal closure by providing contractile forces that pull the contralateral ectodermal sheets together [54, 57, 58]. DC requires DE-Cad-mediated adhesion for ectodermal migration and fusion [59, 60]. To analyze Raskol and DE-Cad dynamics, we conducted time-lapse live imaging of embryos expressing YFP-tagged Raskol and RFP-tagged DE-Cad during DC. Colocalization of Raskol and DE-Cad was observed both at the amnioserosa cell contacts as well as in the dorsal most ectodermal cells at the zippering interface (S3A-D Fig). Raskol and DE-Cad colocalize in multiple *Drosophila* tissues, suggesting that Raskol may be a fundamental regulator of DE-Cad.

Raskol regulates the distribution of polarized actin protrusions

Analysis of Raskol-YFP protein localization in BC clusters revealed that cytoplasmic levels of Raskol were ~2x higher in PCs compared to BCs (S2B Fig and S4A Fig). Similarly, DE-Cad levels were up-regulated in PCs relative to BCs (Fig. 4A) [24] suggesting that Raskol protein expression pattern trends with DE-Cad. Accordingly, *shg* and *raskol* gene expression patterns overlap during embryonic development and both peak at 6-8hrs after egg laying (S4B Fig) [48]. To determine if Raskol is required for maintaining cell adhesions in PCs similar to BCs, we expressed *raskol* RNAi using *unpaired*-GAL4 (*upd*-GAL4) to drive expression specifically in the PCs [61]. Egg chambers were stained for F-actin (phalloidin) and nuclei (DAPI). Expression of control RNAi did not affect cluster adherence; however, *shg* RNAi expression caused cluster disassociation in ~80% egg chambers (Fig 6A, 6B and 6D), similar to a previous report [24]. Expression of *raskol* RNAi in PCs caused BC disassociation in 63% of egg chambers (Fig 6C and 6D), suggesting that Raskol and DE-Cad might function together to promote BC cluster adhesion in both PCs and BCs.

Next, we focused on the Raskol-YFP signal at the leading edge of the BC cluster (Fig 5B and 5D). Here, Raskol colocalized with actin suggesting that it may play a role in actin dynamics. Since Raskol contains a GAP domain and colocalizes with the cortical actin cytoskeleton in BCs, the FE, the amnioserosa and the dorsal most ectodermal cells [55, 60], we sought to determine whether it functions to regulate actin organization in BCs. We stained egg chambers expressing *raskol* RNAi in the BCs under the control of *slbo*-GAL4 driver for F-actin (phalloidin) and nuclei (DAPI) to assess F-actin distribution in the migrating cluster. In control BCs, actin accumulated at the base of protrusions typically oriented in the direction of migration (Fig 6E). In contrast,

downregulation of *raskol* resulted in dramatic formation of multiple ectopic actin patches around the BC cluster (Fig 6F and 6G).

We then performed time-lapse live imaging of BC clusters expressing UAS-lifeact-GFP under the control of *slbo*-GAL4 to analyze protrusion dynamics in more detail. In control egg chambers, we observed protrusions extending primarily from the front of the migrating cluster (Fig 6H, 6J-L; Movie 1). In contrast, when *raskol* was downregulated, protrusions extended indiscriminately around the cluster (Fig 6I-L; Movie 2), consistent with our previous observations. Interestingly, the number of front-oriented protrusions in control and *raskol* RNAi expressing BCs did not differ significantly (Fig 6K). These data suggest that Raskol acts to restrict actin protrusions to the front of the BC cluster, which is critical to regulate BC migration. In addition, *raskol* knockdown caused BC delamination defects (Movie 3) and cluster disassociation (Movie 4) thereby confirming its importance in controlling cell adhesion and providing initial mechanistic insight into its role in regulating actin dynamics.

Discussion

We combined evolution-guided bioinformatics with classical RNAi-based screening in *Drosophila* to identify regulators of DE-Cad-mediated cell adhesion. Our screen uncovered both established and novel regulators of DE-Cad function during BC migration. We demonstrated that one hit, the previously uncharacterized GAP domain containing protein Raskol, colocalizes with DE-Cad and regulates polarized actin dynamics in migrating BCs.

ERC analysis reveals an evolutionary relationship between core components of the AJ

315 The core AJ components *shg*, *α-Cat* and *p120ctn* display high ERC values
316 relative to one another, suggesting that the AJ complex has coevolved under selective
317 pressure. α-Catenin provides the mechanical link between the cadherin-catenin
318 complex and the actin cytoskeleton. Actin linkage is believed to be the original,
319 ancestral function of the adherens junction that provided the foundation for
320 multicellularity [9], so it is not surprising that *shg* and *α-Cat*, given their functional roles,
321 have coevolved. Interestingly, p120-catenin is not essential for cadherin-mediated
322 adhesion in flies [62], though it plays an important role in cadherin endocytosis in flies
323 [63], similar to its established role in vertebrates [64]. Our ERC analysis suggests that
324 shared selective pressures guided the evolution of the p120-catenin and DE-cadherin
325 complex, and we speculate that these pressures may have shaped the range of p120-
326 catenin functions in higher vertebrates.
327 Notably, no significant ERC relationship was observed between *shg* and *arm* or
328 *shg* and other secondary AJ complex genes. While Arm is a core component of the AJ,
329 it also functions as a key transcription factor in the Wnt signaling pathway [28, 29, 65].
330 We speculate that Arm function in Wnt signalling placed additional evolutionary
331 pressures and altered its ERC signature relative to the other AJ genes. Similarly, neither
332 *cno* nor *vinc* showed a strong ERC relationship to AJ genes, possibly reflecting their
333 individual roles in AJ-independent processes [31, 66].
334 A number of genes identified in the *shg* ERC analysis have been implicated in
335 regulating cell adhesion (Fig 1, Table 1). However, many of ERC-identified genes have
336 not been functionally associated with DE-Cad, the AJ or cell adhesion. A previous
337 genomic RNAi screen conducted in *Drosophila* identified multiple regulators of DE-Cad

[43]. Notably, there was little overlap between the two screens. This highlights the potential of ERC analysis as an alternative, unbiased approach to generate a target gene list based solely on the evolutionary rate comparison. However, it is important to conduct secondary screens to validate the function of the target genes in a relevant biological system to eliminate false positives [16, 18, 19]. Also, ERC analysis cannot predict where (e.g., tissue type, cellular component) or when (e.g., developmental stage) a putative interaction will occur. Refinement of the *shg* ERC list based on spatio-temporal expression data can further eliminate false positive hits [19]. Nonetheless, a major advantage of ERC analysis is that genes that would otherwise not arise in a functional or associative genetic screen can be identified.

DE-Cad and its regulators are required for BC migration

BC migration requires coordinated regulation of adhesion and motility [23, 67, 68] and is a good system for testing genes that regulate DE-Cad. BC migration is also an *in vivo* model for metastasis since many morphological characteristics of BCs resemble the invasive behaviour of metastatic cell clusters [68, 69]. However, in contrast to most models of epithelial-to-mesenchymal transition, the detachment of BC cluster requires upregulated levels of DE-Cad [23, 24]. DE-Cad-mediated adhesion between BCs and NCs is required for cluster polarization and directional migration, whereas adhesions between BCs and PCs are required for cluster adherence during migration [24, 25, 70]. Thus, BC migration is a useful system for genetic studies of cell adhesion and offers an opportunity to explore the role of adhesion genes in a relevant disease model [68, 69].

Our secondary genetic screen of *shg* ERC hits revealed potential roles for number of genes in BC migration, including kinases, GTPase regulators, transcription

361 factors and cytoskeletal proteins. A small number of hits have putative or established
362 roles in regulating DE-Cad and/or AJs. For example, PDZ-GEF was shown to colocalize
363 with DE-Cad and function through GTPase Rap1 to regulate DE-Cad at the cell
364 membrane [34, 35]. Hrb98DE is an RNA-binding protein that regulates DE-Cad mRNA
365 processing [32, 33]. Mammalian orthologs of the small GTPase Rab5 regulate E-Cad
366 trafficking [40, 42]. The mammalian homolog of transcription factor CG16952, Btbd7,
367 regulates E-Cad expression [38, 39]. Additionally, genes such as *RhoGAPpp190*, *Stim*,
368 *Appl* and *Rab5* were also identified in functional and proteomics screens of E-Cad [43,
369 44]. We also identified numerous genes that have not been linked to DE-Cad, including
370 raskol, *CG11593*, *babo* and *zormin*. Out of these genes, *raskol*, *CG11593* and *babo*
371 directly regulate DE-Cad levels at the BC-BC contacts (Fig 4). Using *shg* ERC analysis
372 and BC migration as a genetic model we have identified multiple novel genes that
373 function to regulate DE-Cad-mediated cell adhesion in *Drosophila*.

374 **Raskol is a putative regulator of cell adhesion, polarity and actin dynamics**

375 Downregulation of *raskol* caused severe BC cluster disassociation suggesting
376 that Raskol is a critical regulator of BC adhesion. Consistent with this, Raskol
377 colocalized with DE-Cad in multiple cell types and knockdown of *raskol* reduced DE-
378 Cad levels at BC-BC cell contacts. Like *shg*, *raskol* is significantly upregulated in PCs
379 relative to BCs and NCs. The encoded protein contains a highly conserved GAP domain
380 that displays homology towards Ras- and Rho-GAPs, a plekstrin homology (PH) domain
381 and a C2 domain that likely promote its membrane localization [71]. This suggests that,
382 by colocalizing with DE-Cad, Raskol regulates adhesive strength between BCs to
383 maintain cluster adhesion during detachment from the FE and subsequent migration.

384 The mammalian orthologs of Raskol, Rasal2 and Dab2IP, were identified in a screen for
385 RasGAP tumour suppressors [71] and are frequently downregulated in multiple types of
386 cancer cells [53, 72-75]. Rasal2 and Dab2IP are capable of inactivating Ras through
387 inducing GTP hydrolysis through their GAP domain and their downregulation leads to
388 Ras overactivation [76-78]. Furthermore, inactivation of Rasal2 promotes invasive
389 behaviour in a cell migration assay suggesting that Rasal2 has a conserved role in
390 regulating cell adhesion and protrusive behaviour in mammals [71]. Dab2IP was
391 identified in cadherin proximity biotinylation screens in mammalian epithelial cells [44]
392 and mouse neonatal cardiomyocytes [79], further suggesting that the
393 Rasal2/Dab2IP/Raskol family of proteins regulate AJ biology. Nonetheless, the
394 mechanism of their function remains unclear.

395 Our study offers potential insight into Raskol function during collective migration.
396 Epidermal growth factor receptor (EGFR) and PDGF- and VEGF-related receptor (PVR)
397 localize to the leading edge of BC clusters and respond to a presumed gradient of
398 guidance cues originating from the oocyte [67, 80-82]. The BC with the highest levels of
399 EGFR/PVR activation becomes the leader cell and relays a signal to neighboring BCs
400 through the DE-Cad adhesion complex to inhibit protrusion formation at the sides or
401 rear of the cluster [24]. Interestingly, *gurken*, which encodes one of the four ligands for
402 EGFR [81, 83, 84], also appeared on the *shg* ERC list (ERC value 0.62) as did its
403 receptor *Egfr* (epidermal growth factor receptor, ERC value 0.36; S1 Table). The
404 presence of both ligand and receptor suggests that EGF signaling has coevolved with
405 DE-Cad to regulate cell adhesion. The primary GTPase that functions to regulate the
406 directional migration of BC downstream of EGFR and PVR is Rac1, a member of the

Rho GTPase family of proteins. We propose that Raskol, as a GAP, may function to suppress Rac1 signalling in non-leader BCs. Rac1 is expressed in all BCs, but the leader cells exhibit higher activity due to increased activation of EGFR and PVR [24, 80, 85]. Our results show that Raskol, like EGFR, PVR and Rac1 [80, 81, 85], restricts protrusions to the front of migrating BC cluster thus ensuring unidirectional migration. Downregulation of DE-Cad causes disruption in the polarized distribution of Rac1 in BC clusters, suggesting that DE-Cad regulates signaling downstream of EGFR and PVR [24, 86]. Therefore, Rac1 suppression might be achieved through Raskol GAP activity since knockdown of Rac1 or Raskol produce similar protrusion phenotypes [85]. Raskol may buffer the DE-Cad/Rac/actin mechanical feedback loop to regulate cell adhesion and promote collective cell migration. Whether Raskol directly interacts and regulates the GTPase domain of Rac1 remains to be explored.

Raskol localization is polarized with highest levels observed at the apical domain of ectodermal cells, FE cells and PCs. We also observe Raskol localization in the leading protrusion of BC cluster. This suggests that Raskol might regulate actin dynamics at the apical domain of polarized cells. However, Raskol does not directly regulate formation of protrusions since reducing Raskol levels does not affect the prevalence of leading protrusions. We predict that in leading BCs, Raskol limits active Rac1 to the tip of the protrusion to induce localized actin cytoskeletal remodelling. Accordingly, as reported by a Rac1-FRET sensor, high Rac1 activity is limited at the lamellopodial tip in the leading BC [24]. Overall, these data highlights two potential roles of Raskol function: 1) Raskol functions as a putative regulator of cell adhesion, and 2) Raskol regulates actin dynamics of the migrating cluster downstream of receptor

tyrosine kinase signaling in BCs. Future studies dissecting the role of Raskol and other genes identified in our study are expected to offer insight in to the cooperative role of proteins that function along with the AJ to promote cell adhesion and cell migration.

Methods and Materials

Evolutionary Rate Covariance analysis

ERC values were calculated from protein coding sequences from 22 *Drosophila* species: *D. ananassae, D. biarmpies, D. bipectinada, D. elegans, D. erecta, D. eugracilis, D. ficusphila, D. grimshawi, D. kikawaii, D. persimilis, D. pseudoobscura, D. melanogaster, D. miranda, D. mojavensis, D. rhopaloa, D. sechelia, D. simulans, D. suzukii, D. takahashii, D. virilis, D. willistoni,* and *D. yakuba*. Protein coding sequences were downloaded from the Flybase website (http://www.flybase.org/) or the NCBI genome annotation website (https://www.ncbi.nlm.nih.gov/genome/annotation_euk/all/). Initially, coding sequences were evaluated for internal stop codons and the sequence was removed if found. For genes with multiple transcripts, the transcript with the longest sequence size was selected to represent the gene.

Orthology between genes across the multiple species were determined using the Orthofinder algorithm [87]. For each orthogroup, which are sets of genes that are orthologs and/or recent paralogs to each other, we omitted paralogous genes. Only orthogroups that had at least 6 species representation were analyzed further. Gene members of each orthogroup were aligned to each other using the PRANK aligner [88]. The multisequence alignment of each orthogroup was used by the PAML aaml program [89] to estimate the evolutionary rates on a single fixed species topology. A single species topology was estimated using a supertrees approach by combining individual orthogroup topologies that were estimated using RAxML [90]. Trees were combined using the matrix representation method implemented in phytools [91]

ERC was calculated using the branch lengths of each orthogroup. The overall

457 species phylogenetic rates were normalized out for each orthogroup's evolutionary rate,
458 as described previously [18, 19]. Afterwards, ERC was measured as the Kendall's τ
459 correlation coefficients between two orthogroups and their species phylogeny
460 normalized relative rates. ERC was then calculated for all pairwise orthogroup
461 combinations.

462 **Gene ontology analysis**

463 The *Drosophila* gene lists were subjected to GO analysis using Flybase website
464 (http://www.flybase.org/). Homologs of *Drosophila* genes in mammalian genomes were
465 generated using Flybase website (http://www.flybase.org/). A mammalian gene was
466 considered a homolog if the gene was reported by 45% or more algorithms. Mammalian
467 homologs were analyzed for canonical pathway and disease & function enrichment
468 using Ingenuity Pathway Analysis tools
469 (https://www.qiagenbioinformatics.com/products/ingenuity-pathway-analysis/).

470 ***Drosophila melanogaster* strains**

471 All GAL4, reporter TRAP and RNAi stocks were obtained from Bloomington
472 Drosophila Stock Center (BDSC) (S4 Table). *DE-Cad-GFP* and *DE-Cad-mCherry*
473 knock-in stocks were used as E-Cad reporters [49]. s*lbo*-GAL4, UAS-lifeact-GFP, UAS-
474 LacZ stock was generously provided by Jiong Chen (Nanjing University) [92]. Fly stocks
475 were raised on standard yeast-based media at 20°C, unless otherwise noted.

476 **BC migration screen**

477 For BC migration analysis, RNAi-expressing female flies under the control of
478 *slbo*-GAL4 were collected and transferred to vials containing fresh yeast paste and
479 males. Flies were raised at 29ºC for 1-2 days. UAS-GFP was used as a reporter for

480 RNAi expression. Dissected ovaries were fixed in 4% paraformaldehyde in PBS for 20
481 mins and washed 5 times with PBS. Ovaries were mounted on microscope slides in
482 70% glycerol and 20 µm z-stacks were acquired with a 20x objective on Nikon A1
483 scanning confocal microscope.

484 **Immunostaining of egg chambers**

485 1-2 day old females were incubated at 29ºC for 1-2 days in vials with fresh yeast
486 paste and males. Ovaries were dissected, fixed in 4% paraformaldehyde for 20 mins in
487 PBS with 0.1% Triton-X (PBST), washed 5 times with PBST and blocked in normal goat
488 serum (NGS) for 30 mins. For primary antibody staining, ovaries were incubated with
489 Dcad2 antibody (1:100, Developmental Studies Hybridoma Bank) overnight at 4ºC and
490 washed 10 times the next day over 1 hour. Next, ovaries were incubated with Alexa
491 Fluor-conguated secondary antibody (1:150, Thermo Fisher Scientific) and Alexa 647
492 phalloidin (1:150, Thermo Fisher Scientific) for 2 hours. Egg chambers were then
493 incubated in DAPI for 10 mins. Ovaries were washed 5 times in PBST and washed
494 overnight and washed again 5 times next morning. Ovaries were stored and mounted
495 on microscope slide in 70% glycerol and then imaged as described previously.

496 **Live imaging of BC clusters**

497 Male flies containing *slbo*-GAL4, UAS-lifeact-GFP and UAS-LacZ were crossed
498 to UAS-*raskol*-RNAi females. 1-2 day old F1 females were incubated at 29ºC for 1-2
499 days in vials with fresh yeast paste and *slbo*-GAL4, UAS-lifeact-GFP males. Ovaries
500 were dissected for live imaging in imaging media (Schneiders's medium, 15% fetal
501 bovine serum (FBS) and 0.2mg/ml Insulin; Thermo Fisher Scientifc) according to
502 published protocols [22, 93]. 100 µl of imaging media containing egg chambers was

transferred to poly-D-lysine coated Mattek dishes for imaging. 20 µm Z-stacks (1 µm step size) covering the whole migrating border cell cluster were acquired every 2 minutes using a 40x objective on a Nikon A1 scanning confocal microscope.

Live imaging of Raskol-YFP in embryos

Raskol-YFP [51] homozygous female flies were crossed to *DE-Cad-mCherry* [49] homozygous males. Embryos were collected overnight on grape juice agar plates and transferred to microscope slides coated with double-sided tape. Embryos were manually dechorionated and immediately transferred to halocarbon oil on coverslips with the dorsal side facing down. Coverslips were then attached to imaging chambers using double sided tape and imaged using a 60x objective on a Nikon A1 scanning confocal microscope.

Quantification and statistics

Border cell migration defects were quantified as described previously [24]. Stage 10 egg chambers were analysed for each genotype. Border cell position along the migratory path was assigned into one of the following categories: 0-25% (no migration), 25-75% (delayed migration) and 75-100% (completed migration).

To quantify defects in border cell cluster adhesion, we determined the percentage of egg chambers where individual border cells had detached from the cluster.

To quantify DE-Cad levels, linescans across the BC-BC contacts were used to calculate the maximum pixel intensity at the contact in ImageJ. Peak values were then normalized to the peak intensity values of cell-cell contacts between NCs for each egg chamber. One-way ANOVA followed by Mann-Whitney tests were performed to

525 determine significance. At least 22 border cell clusters (3 cell contacts per cluster) were
526 imaged for each genotype.

527 To measure cytoplasmic levels of Raskol, an ROI was drawn in the cytoplasm of
528 polar and border cells and average intensity determined. The ROI intensity was
529 normalized to the average cytoplasmic intensity of Raskol-YFP in the nurse cells. To
530 quantify colocalization of DE-Cad and Raskol, Pearson's correlation coefficient (R) was
531 calculated using the JACop plugin in ImageJ.

532 Ectopic actin patch number was quantified as described [92]. Actin patch present
533 at the base of the leading edge protrusion was excluded from quantification since it is
534 not ectopic. Welch's t-test was performed to statistically compare number of ectopic
535 actin patches between samples.

536 To quantify protrusion direction, we measured protrusions around the BC cluster
537 in 45˚ increments at each frame of the movie (16 frames from 8 movies for each
538 genotype). Protrusions between 315º and 45º angles were considered frontal
539 protrusions; between 45º and 135º and 225º and 315º as middle protrusions; and
540 between 225º and 135º as rear protrusions. Mann-Whitney test was performed to
541 statistically compare number of protrusions between samples.

542 ## Acknowledgements

543 We would like to thank Dr. Jiong Chen for providing *slbo*-lifeact-GFP stock and
544 Bloomington Drosophila Stock Center for providing GAL4 and RNAi stocks. We also
545 thank members of the Kwiatkowski lab for critical feedback on the manuscript.

546

References

1. Harris TJ, Tepass U. Adherens junctions: from molecules to morphogenesis. Nature reviews Molecular cell biology. 2010;11(7):502-14. doi: 10.1038/nrm2927. PubMed PMID: 20571587.

2. Mege RM, Ishiyama N. Integration of Cadherin Adhesion and Cytoskeleton at Adherens Junctions. Cold Spring Harb Perspect Biol. 2017;9(5). Epub 2017/01/18. doi: 10.1101/cshperspect.a028738. PubMed PMID: 28096263.

3. Yap AS, Gomez GA, Parton RG. Adherens Junctions Revisualized: Organizing Cadherins as Nanoassemblies. Dev Cell. 2015;35(1):12-20. Epub 2015/10/16. doi: 10.1016/j.devcel.2015.09.012. PubMed PMID: 26460944.

4. Brunet T, King N. The Origin of Animal Multicellularity and Cell Differentiation. Dev Cell. 2017;43(2):124-40. Epub 2017/10/25. doi: 10.1016/j.devcel.2017.09.016. PubMed PMID: 29065305; PubMed Central PMCID: PMCPMC6089241.

5. Miller PW, Clarke DN, Weis WI, Lowe CJ, Nelson WJ. The evolutionary origin of epithelial cell-cell adhesion mechanisms. Curr Top Membr. 2013;72:267-311. Epub 2013/11/12. doi: 10.1016/B978-0-12-417027-8.00008-8. PubMed PMID: 24210433; PubMed Central PMCID: PMCPMC4118598.

6. Hulpiau P, Gul IS, van Roy F. New insights into the evolution of metazoan cadherins and catenins. Prog Mol Biol Transl Sci. 2013;116:71-94. Epub 2013/03/14. doi: 10.1016/B978-0-12-394311-8.00004-2. PubMed PMID: 23481191.

7. Miller PW, Pokutta S, Mitchell JM, Chodaparambil JV, Clarke DN, Nelson WJ, et al. Analysis of a vinculin homolog in a sponge (phylum Porifera) reveals that vertebrate-like cell adhesions emerged early in animal evolution. J Biol Chem. 2018;293(30):11674-86. Epub 2018/06/09. doi: 10.1074/jbc.RA117.001325. PubMed PMID: 29880641; PubMed Central PMCID: PMCPMC6066325.

8. Murray PS, Zaidel-Bar R. Pre-metazoan origins and evolution of the cadherin adhesome. Biol Open. 2014;3(12):1183-95. Epub 2014/11/15. doi: 10.1242/bio.20149761. PubMed PMID: 25395670; PubMed Central PMCID: PMCPMC4265756.

9. Rubsam M, Broussard JA, Wickstrom SA, Nekrasova O, Green KJ, Niessen CM. Adherens Junctions and Desmosomes Coordinate Mechanics and Signaling to Orchestrate Tissue Morphogenesis and Function: An Evolutionary Perspective. Cold Spring Harb Perspect Biol. 2017. Epub 2017/09/13. doi: 10.1101/cshperspect.a029207. PubMed PMID: 28893859.

10. Meng W, Takeichi M. Adherens junction: molecular architecture and regulation. Cold Spring Harb Perspect Biol. 2009;1(6):a002899. doi:

583 10.1101/cshperspect.a002899. PubMed PMID: 20457565; PubMed Central PMCID:
584 PMC2882120.

585 11. Menke A, Giehl K. Regulation of adherens junctions by Rho GTPases and p120-
586 catenin. Archives of biochemistry and biophysics. 2012;524(1):48-55. doi:
587 10.1016/j.abb.2012.04.019. PubMed PMID: 22583808.

588 12. Bertocchi C, Vaman Rao M, Zaidel-Bar R. Regulation of adherens junction
589 dynamics by phosphorylation switches. Journal of signal transduction.
590 2012;2012:125295. doi: 10.1155/2012/125295. PubMed PMID: 22848810; PubMed
591 Central PMCID: PMC3403498.

592 13. Padmanabhan A, Rao MV, Wu Y, Zaidel-Bar R. Jack of all trades: functional
593 modularity in the adherens junction. Curr Opin Cell Biol. 2015;36:32-40. Epub
594 2015/07/21. doi: 10.1016/j.ceb.2015.06.008. PubMed PMID: 26189061.

595 14. Garcia MA, Nelson WJ, Chavez N. Cell-Cell Junctions Organize Structural and
596 Signaling Networks. Cold Spring Harb Perspect Biol. 2018;10(4). Epub 2017/06/11. doi:
597 10.1101/cshperspect.a029181. PubMed PMID: 28600395; PubMed Central PMCID:
598 PMCPMC5773398.

599 15. Clark NL, Alani E, Aquadro CF. Evolutionary rate covariation in meiotic proteins
600 results from fluctuating evolutionary pressure in yeasts and mammals. Genetics.
601 2013;193(2):529-38. doi: 10.1534/genetics.112.145979. PubMed PMID: 23183665;
602 PubMed Central PMCID: PMC3567741.

603 16. Findlay GD, Sitnik JL, Wang W, Aquadro CF, Clark NL, Wolfner MF. Evolutionary
604 rate covariation identifies new members of a protein network required for Drosophila
605 melanogaster female post-mating responses. PLoS genetics. 2014;10(1):e1004108.
606 doi: 10.1371/journal.pgen.1004108. PubMed PMID: 24453993; PubMed Central
607 PMCID: PMC3894160.

608 17. Wolfe NW, Clark NL. ERC analysis: web-based inference of gene function via
609 evolutionary rate covariation. Bioinformatics. 2015;31(23):3835-7. doi:
610 10.1093/bioinformatics/btv454. PubMed PMID: 26243019; PubMed Central PMCID:
611 PMC4751245.

612 18. Priedigkeit N, Wolfe N, Clark NL. Evolutionary signatures amongst disease
613 genes permit novel methods for gene prioritization and construction of informative gene-
614 based networks. PLoS genetics. 2015;11(2):e1004967. doi:
615 10.1371/journal.pgen.1004967. PubMed PMID: 25679399; PubMed Central PMCID:
616 PMC4334549.

617 19. Clark NL, Alani E, Aquadro CF. Evolutionary rate covariation reveals shared
618 functionality and coexpression of genes. Genome research. 2012;22(4):714-20. doi:
619 10.1101/gr.132647.111. PubMed PMID: 22287101; PubMed Central PMCID:
620 PMC3317153.

621 20. Godin SK, Meslin C, Kabbinavar F, Bratton-Palmer DS, Hornack C, Mihalevic
622 MJ, et al. Evolutionary and functional analysis of the invariant SWIM domain in the
623 conserved Shu2/SWS1 protein family from Saccharomyces cerevisiae to Homo
624 sapiens. Genetics. 2015;199(4):1023-33. doi: 10.1534/genetics.114.173518. PubMed
625 PMID: 25659377; PubMed Central PMCID: PMC4391554.

626 21. Ziegler AB, Augustin H, Clark NL, Berthelot-Grosjean M, Simonnet MM, Steinert
627 JR, et al. The Amino Acid Transporter Jhl-21 Coevolves with Glutamate Receptors,
628 Impacts NMJ Physiology, and Influences Locomotor Activity in Drosophila Larvae.
629 Scientific reports. 2016;6:19692. doi: 10.1038/srep19692. PubMed PMID: 26805723;
630 PubMed Central PMCID: PMC4726445.

631 22. Prasad M, Wang X, He L, Cai D, Montell DJ. Border Cell Migration: A Model
632 System for Live Imaging and Genetic Analysis of Collective Cell Movement. Methods in
633 molecular biology. 2015;1328:89-97. doi: 10.1007/978-1-4939-2851-4_6. PubMed
634 PMID: 26324431; PubMed Central PMCID: PMC4762686.

635 23. Montell DJ, Yoon WH, Starz-Gaiano M. Group choreography: mechanisms
636 orchestrating the collective movement of border cells. Nature reviews Molecular cell
637 biology. 2012;13(10):631-45. doi: 10.1038/nrm3433. PubMed PMID: 23000794;
638 PubMed Central PMCID: PMC4099007.

639 24. Cai D, Chen SC, Prasad M, He L, Wang X, Choesmel-Cadamuro V, et al.
640 Mechanical feedback through E-cadherin promotes direction sensing during collective
641 cell migration. Cell. 2014;157(5):1146-59. doi: 10.1016/j.cell.2014.03.045. PubMed
642 PMID: 24855950; PubMed Central PMCID: PMC4118667.

643 25. Niewiadomska P, Godt D, Tepass U. DE-Cadherin is required for intercellular
644 motility during Drosophila oogenesis. The Journal of cell biology. 1999;144(3):533-47.
645 PubMed PMID: 9971747; PubMed Central PMCID: PMC2132905.

646 26. Fulga TA, Rorth P. Invasive cell migration is initiated by guided growth of long
647 cellular extensions. Nature cell biology. 2002;4(9):715-9. Epub 2002/08/29. doi:
648 10.1038/ncb848. PubMed PMID: 12198500.

649 27. Harris TJ. Adherens junction assembly and function in the Drosophila embryo.
650 International review of cell and molecular biology. 2012;293:45-83. doi: 10.1016/B978-
651 0-12-394304-0.00007-5. PubMed PMID: 22251558.

652 28. Mosimann C, Hausmann G, Basler K. Beta-catenin hits chromatin: regulation of
653 Wnt target gene activation. Nature reviews Molecular cell biology. 2009;10(4):276-86.
654 doi: 10.1038/nrm2654. PubMed PMID: 19305417.

655 29. Clevers H, Nusse R. Wnt/beta-catenin signaling and disease. Cell.
656 2012;149(6):1192-205. doi: 10.1016/j.cell.2012.05.012. PubMed PMID: 22682243.

657 30. Atherton P, Stutchbury B, Jethwa D, Ballestrem C. Mechanosensitive
658 components of integrin adhesions: Role of vinculin. Experimental cell research.

659 2016;343(1):21-7. doi: 10.1016/j.yexcr.2015.11.017. PubMed PMID: 26607713;
660 PubMed Central PMCID: PMC4856733.

661 31. Mandai K, Rikitake Y, Shimono Y, Takai Y. Afadin/AF-6 and canoe: roles in cell
662 adhesion and beyond. Prog Mol Biol Transl Sci. 2013;116:433-54. doi: 10.1016/B978-0-
663 12-394311-8.00019-4. PubMed PMID: 23481206.

664 32. Kourtidis A, Ngok SP, Pulimeno P, Feathers RW, Carpio LR, Baker TR, et al.
665 Distinct E-cadherin-based complexes regulate cell behaviour through miRNA
666 processing or Src and p120 catenin activity. Nature cell biology. 2015;17(9):1145-57.
667 doi: 10.1038/ncb3227. PubMed PMID: 26302406; PubMed Central PMCID:
668 PMC4975377.

669 33. Ji Y, Tulin AV. Poly(ADP-ribose) controls DE-cadherin-dependent stem cell
670 maintenance and oocyte localization. Nature communications. 2012;3:760. doi:
671 10.1038/ncomms1759. PubMed PMID: 22453833; PubMed Central PMCID:
672 PMC3319983.

673 34. Boettner B, Van Aelst L. The Rap GTPase activator Drosophila PDZ-GEF
674 regulates cell shape in epithelial migration and morphogenesis. Molecular and cellular
675 biology. 2007;27(22):7966-80. doi: 10.1128/MCB.01275-07. PubMed PMID: 17846121;
676 PubMed Central PMCID: PMC2169160.

677 35. Spahn P, Ott A, Reuter R. The PDZ-GEF protein Dizzy regulates the
678 establishment of adherens junctions required for ventral furrow formation in Drosophila.
679 Journal of cell science. 2012;125(Pt 16):3801-12. doi: 10.1242/jcs.101196. PubMed
680 PMID: 22553205.

681 36. Rudini N, Felici A, Giampietro C, Lampugnani M, Corada M, Swirsding K, et al.
682 VE-cadherin is a critical endothelial regulator of TGF-beta signalling. The EMBO journal.
683 2008;27(7):993-1004. doi: 10.1038/emboj.2008.46. PubMed PMID: 18337748; PubMed
684 Central PMCID: PMC2323269.

685 37. Fornetti J, Flanders KC, Henson PM, Tan AC, Borges VF, Schedin P. Mammary
686 epithelial cell phagocytosis downstream of TGF-beta3 is characterized by adherens
687 junction reorganization. Cell death and differentiation. 2016;23(2):185-96. doi:
688 10.1038/cdd.2015.82. PubMed PMID: 26113040; PubMed Central PMCID:
689 PMC4716300.

690 38. Onodera T, Sakai T, Hsu JC, Matsumoto K, Chiorini JA, Yamada KM. Btbd7
691 regulates epithelial cell dynamics and branching morphogenesis. Science.
692 2010;329(5991):562-5. doi: 10.1126/science.1191880. PubMed PMID: 20671187;
693 PubMed Central PMCID: PMC3412157.

694 39. Fan C, Miao Y, Zhang X, Liu D, Jiang G, Lin X, et al. Btbd7 contributes to
695 reduced E-cadherin expression and predicts poor prognosis in non-small cell lung
696 cancer. BMC cancer. 2014;14:704. doi: 10.1186/1471-2407-14-704. PubMed PMID:
697 25253020; PubMed Central PMCID: PMC4189533.

698 40. Yang J, Yao W, Qian G, Wei Z, Wu G, Wang G. Rab5-mediated VE-cadherin
699 internalization regulates the barrier function of the lung microvascular endothelium.
700 Cellular and molecular life sciences : CMLS. 2015;72(24):4849-66. doi:
701 10.1007/s00018-015-1973-4. PubMed PMID: 26112597; PubMed Central PMCID:
702 PMC4827161.

703 41. Woichansky I, Beretta CA, Berns N, Riechmann V. Three mechanisms control E-
704 cadherin localization to the zonula adherens. Nature communications. 2016;7:10834.
705 doi: 10.1038/ncomms10834. PubMed PMID: 26960923; PubMed Central PMCID:
706 PMC4792928.

707 42. Saitoh S, Maruyama T, Yako Y, Kajita M, Fujioka Y, Ohba Y, et al. Rab5-
708 regulated endocytosis plays a crucial role in apical extrusion of transformed cells.
709 Proceedings of the National Academy of Sciences of the United States of America.
710 2017;114(12):E2327-E36. doi: 10.1073/pnas.1602349114. PubMed PMID: 28270608;
711 PubMed Central PMCID: PMC5373379.

712 43. Toret CP, D'Ambrosio MV, Vale RD, Simon MA, Nelson WJ. A genome-wide
713 screen identifies conserved protein hubs required for cadherin-mediated cell-cell
714 adhesion. The Journal of cell biology. 2014;204(2):265-79. doi: 10.1083/jcb.201306082.
715 PubMed PMID: 24446484; PubMed Central PMCID: PMC3897182.

716 44. Guo Z, Neilson LJ, Zhong H, Murray PS, Zanivan S, Zaidel-Bar R. E-cadherin
717 interactome complexity and robustness resolved by quantitative proteomics. Science
718 signaling. 2014;7(354):rs7. doi: 10.1126/scisignal.2005473. PubMed PMID: 25468996;
719 PubMed Central PMCID: PMC4972397.

720 45. Van Itallie CM, Tietgens AJ, Aponte A, Fredriksson K, Fanning AS, Gucek M, et
721 al. Biotin ligase tagging identifies proteins proximal to E-cadherin, including lipoma
722 preferred partner, a regulator of epithelial cell-cell and cell-substrate adhesion. Journal
723 of cell science. 2014;127(Pt 4):885-95. Epub 2013/12/18. doi: 10.1242/jcs.140475.
724 PubMed PMID: 24338363; PubMed Central PMCID: PMCPMC3924204.

725 46. Montell DJ, Rorth P, Spradling AC. slow border cells, a locus required for a
726 developmentally regulated cell migration during oogenesis, encodes Drosophila C/EBP.
727 Cell. 1992;71(1):51-62. PubMed PMID: 1394432.

728 47. Rorth P, Szabo K, Bailey A, Laverty T, Rehm J, Rubin GM, et al. Systematic
729 gain-of-function genetics in Drosophila. Development. 1998;125(6):1049-57. PubMed
730 PMID: 9463351.

731 48. Contrino S, Smith RN, Butano D, Carr A, Hu F, Lyne R, et al. modMine: flexible
732 access to modENCODE data. Nucleic acids research. 2012;40(Database issue):D1082-
733 8. doi: 10.1093/nar/gkr921. PubMed PMID: 22080565; PubMed Central PMCID:
734 PMC3245176.

735 49. Huang J, Zhou W, Dong W, Watson AM, Hong Y. From the Cover: Directed,
736 efficient, and versatile modifications of the Drosophila genome by genomic engineering.

737 Proceedings of the National Academy of Sciences of the United States of America.
738 2009;106(20):8284-9. doi: 10.1073/pnas.0900641106. PubMed PMID: 19429710;
739 PubMed Central PMCID: PMC2688891.

740 50. Cho KS, Lee JH, Kim S, Kim D, Koh H, Lee J, et al. Drosophila phosphoinositide-
741 dependent kinase-1 regulates apoptosis and growth via the phosphoinositide 3-kinase-
742 dependent signaling pathway. Proceedings of the National Academy of Sciences of the
743 United States of America. 2001;98(11):6144-9. doi: 10.1073/pnas.101596998. PubMed
744 PMID: 11344272; PubMed Central PMCID: PMC33436.

745 51. Lye CM, Naylor HW, Sanson B. Subcellular localisations of the CPTI collection of
746 YFP-tagged proteins in Drosophila embryos. Development. 2014;141(20):4006-17. doi:
747 10.1242/dev.111310. PubMed PMID: 25294944; PubMed Central PMCID:
748 PMC4197698.

749 52. Thul PJ, Akesson L, Wiking M, Mahdessian D, Geladaki A, Ait Blal H, et al. A
750 subcellular map of the human proteome. Science. 2017;356(6340). doi:
751 10.1126/science.aal3321. PubMed PMID: 28495876.

752 53. Jia Z, Liu W, Gong L, Xiao Z. Downregulation of RASAL2 promotes the
753 proliferation, epithelial-mesenchymal transition and metastasis of colorectal cancer
754 cells. Oncology letters. 2017;13(3):1379-85. doi: 10.3892/ol.2017.5581. PubMed PMID:
755 28454265; PubMed Central PMCID: PMC5403410.

756 54. Hayes P, Solon J. Drosophila dorsal closure: An orchestra of forces to zip shut
757 the embryo. Mechanisms of development. 2017;144(Pt A):2-10. doi:
758 10.1016/j.mod.2016.12.005. PubMed PMID: 28077304.

759 55. Kiehart DP, Crawford JM, Aristotelous A, Venakides S, Edwards GS. Cell Sheet
760 Morphogenesis: Dorsal Closure in Drosophila melanogaster as a Model System. Annual
761 review of cell and developmental biology. 2017;33:169-202. doi: 10.1146/annurev-
762 cellbio-111315-125357. PubMed PMID: 28992442.

763 56. Heisenberg CP. Dorsal closure in Drosophila: cells cannot get out of the tight
764 spot. BioEssays : news and reviews in molecular, cellular and developmental biology.
765 2009;31(12):1284-7. doi: 10.1002/bies.200900109. PubMed PMID: 19882683.

766 57. Kiehart DP, Galbraith CG, Edwards KA, Rickoll WL, Montague RA. Multiple
767 forces contribute to cell sheet morphogenesis for dorsal closure in Drosophila. The
768 Journal of cell biology. 2000;149(2):471-90. PubMed PMID: 10769037; PubMed Central
769 PMCID: PMC2175161.

770 58. Lynch HE, Crews SM, Rosenthal B, Kim E, Gish R, Echiverri K, et al. Cellular
771 mechanics of germ band retraction in Drosophila. Developmental biology.
772 2013;384(2):205-13. doi: 10.1016/j.ydbio.2013.10.005. PubMed PMID: 24135149;
773 PubMed Central PMCID: PMC3856716.

774 59. Gorfinkiel N, Arias AM. Requirements for adherens junction components in the
775 interaction between epithelial tissues during dorsal closure in Drosophila. Journal of cell
776 science. 2007;120(18):3289-98. doi: 10.1242/jcs.010850. PubMed PMID:
777 WOS:000249559400015.

778 60. Duque J, Gorfinkiel N. Integration of actomyosin contractility with cell-cell
779 adhesion during dorsal closure. Development. 2016;143(24):4676-86. doi:
780 10.1242/dev.136127. PubMed PMID: WOS:000393454600012.

781 61. Beccari S, Teixeira L, Rorth P. The JAK/STAT pathway is required for border cell
782 migration during Drosophila oogenesis. Mechanisms of development. 2002;111(1-
783 2):115-23. Epub 2002/01/24. PubMed PMID: 11804783.

784 62. Myster SH, Cavallo R, Anderson CT, Fox DT, Peifer M. Drosophila p120catenin
785 plays a supporting role in cell adhesion but is not an essential adherens junction
786 component. Journal of Cell Biology. 2003;160(3):433-49. doi: 10.1083/jcb.200211083.
787 PubMed PMID: WOS:000180840800017.

788 63. Bulgakova NA, Brown NH. Drosophila p120-catenin is crucial for endocytosis of
789 the dynamic E-cadherin-Bazooka complex. Journal of cell science. 2016;129(3):477-82.
790 doi: 10.1242/jcs.177527. PubMed PMID: WOS:000369505600004.

791 64. Kourtidis A, Ngok SP, Anastasiadis PZ. p120 catenin: an essential regulator of
792 cadherin stability, adhesion-induced signaling, and cancer progression. Prog Mol Biol
793 Transl Sci. 2013;116:409-32. Epub 2013/03/14. doi: 10.1016/B978-0-12-394311-
794 8.00018-2. PubMed PMID: 23481205; PubMed Central PMCID: PMCPMC4960658.

795 65. Moon RT, Kohn AD, De Ferrari GV, Kaykas A. WNT and beta-catenin signalling:
796 diseases and therapies. Nature reviews Genetics. 2004;5(9):691-701. doi:
797 10.1038/nrg1427. PubMed PMID: 15372092.

798 66. Bays JL, DeMali KA. Vinculin in cell-cell and cell-matrix adhesions. Cellular and
799 molecular life sciences : CMLS. 2017;74(16):2999-3009. Epub 2017/04/13. doi:
800 10.1007/s00018-017-2511-3. PubMed PMID: 28401269; PubMed Central PMCID:
801 PMCPMC5501900.

802 67. Cai D, Dai W, Prasad M, Luo J, Gov NS, Montell DJ. Modeling and analysis of
803 collective cell migration in an in vivo three-dimensional environment. Proceedings of the
804 National Academy of Sciences of the United States of America. 2016;113(15):E2134-
805 41. doi: 10.1073/pnas.1522656113. PubMed PMID: 27035964; PubMed Central
806 PMCID: PMC4839456.

807 68. Friedl P, Gilmour D. Collective cell migration in morphogenesis, regeneration and
808 cancer. Nature reviews Molecular cell biology. 2009;10(7):445-57. doi:
809 10.1038/nrm2720. PubMed PMID: 19546857.

69. Stuelten CH, Parent CA, Montell DJ. Cell motility in cancer invasion and metastasis: insights from simple model organisms. Nature reviews Cancer. 2018;18(5):296-312. doi: 10.1038/nrc.2018.15. PubMed PMID: 29546880.

70. Geisbrecht ER, Sawant K, Su Y, Liu ZC, Silver DL, Burtscher A, et al. Genetic interaction screens identify a role for hedgehog signaling in Drosophila border cell migration. Developmental dynamics : an official publication of the American Association of Anatomists. 2013;242(5):414-31. doi: 10.1002/dvdy.23926. PubMed PMID: 23335293; PubMed Central PMCID: PMC3721345.

71. McLaughlin SK, Olsen SN, Dake B, De Raedt T, Lim E, Bronson RT, et al. The RasGAP gene, RASAL2, is a tumor and metastasis suppressor. Cancer cell. 2013;24(3):365-78. doi: 10.1016/j.ccr.2013.08.004. PubMed PMID: 24029233; PubMed Central PMCID: PMC3822334.

72. Sun L, Yao Y, Lu T, Shang Z, Zhan S, Shi W, et al. DAB2IP Downregulation Enhances the Proliferation and Metastasis of Human Gastric Cancer Cells by Derepressing the ERK1/2 Pathway. Gastroenterology research and practice. 2018;2018:2968252. doi: 10.1155/2018/2968252. PubMed PMID: 29743885; PubMed Central PMCID: PMC5884246.

73. Liu L, Xu C, Hsieh JT, Gong J, Xie D. DAB2IP in cancer. Oncotarget. 2016;7(4):3766-76. doi: 10.18632/oncotarget.6501. PubMed PMID: 26658103; PubMed Central PMCID: PMC4826168.

74. Dote H, Toyooka S, Tsukuda K, Yano M, Ouchida M, Doihara H, et al. Aberrant promoter methylation in human DAB2 interactive protein (hDAB2IP) gene in breast cancer. Clinical cancer research : an official journal of the American Association for Cancer Research. 2004;10(6):2082-9. PubMed PMID: 15041729.

75. Huang Y, Zhao M, Xu H, Wang K, Fu Z, Jiang Y, et al. RASAL2 down-regulation in ovarian cancer promotes epithelial-mesenchymal transition and metastasis. Oncotarget. 2014;5(16):6734-45. doi: 10.18632/oncotarget.2244. PubMed PMID: 25216515; PubMed Central PMCID: PMC4196159.

76. Hui K, Wu S, Yue Y, Gu Y, Guan B, Wang X, et al. RASAL2 inhibits tumor angiogenesis via p-AKT/ETS1 signaling in bladder cancer. Cellular signalling. 2018;48:38-44. doi: 10.1016/j.cellsig.2018.04.006. PubMed PMID: 29702203.

77. Noto S, Maeda T, Hattori S, Inazawa J, Imamura M, Asaka M, et al. A novel human RasGAP-like gene that maps within the prostate cancer susceptibility locus at chromosome 1q25. FEBS letters. 1998;441(1):127-31. PubMed PMID: 9877179.

78. Maertens O, Cichowski K. An expanding role for RAS GTPase activating proteins (RAS GAPs) in cancer. Advances in biological regulation. 2014;55:1-14. doi: 10.1016/j.jbior.2014.04.002. PubMed PMID: 24814062.

847 79. Li Y, Merkel CD, Yang X, Heier JA, Cantrell PS, Sun M, et al. The N-cadherin
848 interactome in primary cardiomyocytes as defined by quantitative proximity proteomics.
849 2018. doi: 10.1101/348953 %J bioRxiv.

850 80. Bianco A, Poukkula M, Cliffe A, Mathieu J, Luque CM, Fulga TA, et al. Two
851 distinct modes of guidance signalling during collective migration of border cells. Nature.
852 2007;448(7151):362-5. doi: 10.1038/nature05965. PubMed PMID: 17637670.

853 81. McDonald JA, Pinheiro EM, Kadlec L, Schupbach T, Montell DJ. Multiple EGFR
854 ligands participate in guiding migrating border cells. Developmental biology.
855 2006;296(1):94-103. doi: 10.1016/j.ydbio.2006.04.438. PubMed PMID: 16712835.

856 82. Duchek P, Somogyi K, Jekely G, Beccari S, Rorth P. Guidance of cell migration
857 by the Drosophila PDGF/VEGF receptor. Cell. 2001;107(1):17-26. PubMed PMID:
858 11595182.

859 83. Goentoro LA, Reeves GT, Kowal CP, Martinelli L, Schupbach T, Shvartsman SY.
860 Quantifying the Gurken morphogen gradient in Drosophila oogenesis. Dev Cell.
861 2006;11(2):263-72. doi: 10.1016/j.devcel.2006.07.004. PubMed PMID: 16890165;
862 PubMed Central PMCID: PMC4091837.

863 84. Shilo BZ. Signaling by the Drosophila epidermal growth factor receptor pathway
864 during development. Experimental cell research. 2003;284(1):140-9. PubMed PMID:
865 12648473.

866 85. Wang X, He L, Wu YI, Hahn KM, Montell DJ. Light-mediated activation reveals a
867 key role for Rac in collective guidance of cell movement in vivo. Nature cell biology.
868 2010;12(6):591-7. doi: 10.1038/ncb2061. PubMed PMID: 20473296; PubMed Central
869 PMCID: PMC2929827.

870 86. Ridley AJ. Rho GTPase signalling in cell migration. Curr Opin Cell Biol.
871 2015;36:103-12. doi: 10.1016/j.ceb.2015.08.005. PubMed PMID: 26363959; PubMed
872 Central PMCID: PMC4728192.

873 87. Emms DM, Kelly S. OrthoFinder: solving fundamental biases in whole genome
874 comparisons dramatically improves orthogroup inference accuracy. Genome biology.
875 2015;16:157. doi: 10.1186/s13059-015-0721-2. PubMed PMID: 26243257; PubMed
876 Central PMCID: PMC4531804.

877 88. Loytynoja A, Goldman N. Phylogeny-aware gap placement prevents errors in
878 sequence alignment and evolutionary analysis. Science. 2008;320(5883):1632-5. doi:
879 10.1126/science.1158395. PubMed PMID: 18566285.

880 89. Yang ZH. PAML 4: Phylogenetic analysis by maximum likelihood. Mol Biol Evol.
881 2007;24(8):1586-91. doi: 10.1093/molbev/msm088. PubMed PMID:
882 WOS:000248848400003.

883 90. Stamatakis A. RAxML version 8: a tool for phylogenetic analysis and post-
884 analysis of large phylogenies. Bioinformatics. 2014;30(9):1312-3. doi:
885 10.1093/bioinformatics/btu033. PubMed PMID: WOS:000336095100024.

886 91. Revell LJ. phytools: an R package for phylogenetic comparative biology (and
887 other things). Methods Ecol Evol. 2012;3(2):217-23. doi: 10.1111/j.2041-
888 210X.2011.00169.x. PubMed PMID: WOS:000302538500001.

889 92. Wang H, Qiu Z, Xu Z, Chen SJ, Luo J, Wang X, et al. aPKC is a key polarity
890 determinant in coordinating the function of three distinct cell polarities during collective
891 migration. Development. 2018;145(9). doi: 10.1242/dev.158444. PubMed PMID:
892 29636381.

893 93. Prasad M, Jang AC, Starz-Gaiano M, Melani M, Montell DJ. A protocol for
894 culturing Drosophila melanogaster stage 9 egg chambers for live imaging. Nature
895 protocols. 2007;2(10):2467-73. doi: 10.1038/nprot.2007.363. PubMed PMID: 17947988.

896

897

Figure Legends

Fig 1. Gene ontology enrichment analysis for genes identified in *shg* ERC analysis. A. ERC analysis reveals an evolutionary relationship between *shg*, *α-cat* and *p120ctn*. B. Genes from the *shg* list with ERC values ≥ 0.4 are enriched for genes that encode plasma membrane and cell periphery proteins. C. *shg* ERC list is enriched for genes with established roles in regulating biological processes that require cadherin-mediated adhesion. D. Human orthologs of the *shg* ERC list are involved in remodeling of epithelial AJs and multiple canonical pathways including RhoA, TGF-β, PTEN and AJ signaling.

Fig 2. *shg* ERC genes regulate BC migration. A. Cartoon representation of BC migration during egg chamber development. BC, border cell; PC, polar cell; NC, nurse cell; FE, follicular epithelium; A, anterior; P, posterior. B-G. Representative images of egg chambers expressing UAS-GFP and UAS-RNAi for control (luciferase) (B), *shg* (C), *Pdk1* (D), *babo* (E), *CG42684* (F) or *CG16952* (G) under the control of *slbo*-GAL4. White arrow indicates BC cluster position. Yellow triangles mark FE retraction border. Maximum projections of 20 μm z-stacks are shown. Posterior is to the right in all images. H. Border cell migration scoring classes. I-K. Percentage of egg chambers in each class displaying migration defects in AJ-related genes (I), *shg* ERC target genes (J) and random negative control genes (K). Red 0-25%, yellow 25-75% and green 75-100%. N values are listed in S5 Table. Scale bar in G is 50 μm and applies to B-G.

Fig 3. *shg* ERC genes maintain BC adhesion during migration. A-F. Egg chambers expressing UAS-GFP and UAS-RNAi for control (A), *α-Cat* (B), *CG42684* (C), *PDZ-GEF* (D), *CG16952* (E) or *CG11593* (F). White arrows mark disassociated BCs. White

arrowheads mark BC cluster adjacent to oocyte. Yellow triangles mark the FE retraction border. Maximum projections of 20 μm z-stacks are shown. G-I. Percentage of egg chambers displaying a cluster disassociation phenotype in AJ genes (G), *shg* ERC target genes (H) and random negative control genes (I). Scale bar in F is 50 μm and applies to A-F.

Fig 4. *shg* ERC genes regulate DE-Cadherin levels in BCs. A-G. Representative images of BC clusters stained for nuclei (blue) and expressing DE-Cad-GFP and control (A,), *shg* (B), *CG42684* (C), *CG16952* (D), *CG11593* (E), *Pdk1* (F) or *babo* (G) RNAi under the control of *slbo*-GAL4. White arrows mark BC-BC contacts. PCs are outlined by a dashed line. Maximum projections of 5 μm z-stacks are shown. H. Quantification of DE-Cad levels at BC-BC contacts in control (n=69), *shg* (n=66), *CG42684* (n=72), *CG16952* (n=69), *CG11593*(n=69), *Pdk1*(n=66) and *babo* (n=69) RNAi-expressing BCs. **** - $p<0.0001$, *** - $p<0.001$. Error bars represent mean ± SD. Scale bar in G is 10 μm and applies to A-G.

Fig 5. Raskol localizes to BC contacts. A-B. Egg chambers expressing Raskol-YFP and stained for F-actin (red) at stage 8 (A) and stage 9 (B). C-D. Egg chamber expressing Raskol-YFP and stained with DE-Cad (red) at stage 8 (C) and stage 9 (D). Yellow triangles indicate the apical side of PCs. Purple triangles mark cell-cell contacts. White triangles mark Raskol localization in the leading protrusion. FE – follicular epithelium. Maximum projections of 5 μm z-stacks are shown. Scale bar in D is 10 μm and applies to A-D.

Fig 6. Raskol regulates actin organization in migrating BC clusters. A-C. Representative images of egg chambers stained for F-actin (green) and nuclei (blue)

944 expressing control RNAi (A), *shg* RNAi (B) and *raskol* RNAi (C) in PCs using *upd*-GAL4.
945 Asterisks mark the final position of the BC cluster adjacent to the oocyte. Arrows mark
946 disassociated BC cells along the migratory path. Maximum projections of 10 μm stacks
947 z-stacks are shown. D. Quantification of the cluster disassociation phenotype in control,
948 *shg* and *raskol* RNAi-expressing BCs ($p<0.0001$). E-F. BC cluster expressing control
949 RNAi (E) and *raskol* RNAi (F) under the control of *slbo*-GAL4 and stained for F-actin
950 (red) and nuclei (blue). A white arrow marks the actin patch at the leading protrusion.
951 White arrowheads mark ectopic actin patches around the BC cluster. G. Quantification
952 of ectopic actin patches in control (n=30) and *raskol* (n=39) RNAi BC clusters
953 ($p<0.0001$). H-I. Time-lapse images of migrating cluster expressing lifeact-GFP and
954 control RNAi (H, n=8) or *raskol* RNAi (I, n=8) in BCs. White arrows mark the leading
955 protrusion. Red triangles mark ectopic protrusions. f - front, m - middle and r - rear. J.
956 Radar maps showing the distribution of protrusions around the BC cluster. 0˚ is the
957 direction of migration. K. Number of front-oriented protrusions per frame observed in
958 control and *raskol* RNAi expressing clusters. $p=0.71$. L. Number of protrusions per
959 frame at the middle and rear of control RNAi and *raskol* RNAi-expressing clusters
960 ($p=0.0002$). Scale bar in C is 10 μm and applies to A-C. Scale bar in panel F is 10 μm
961 and applies to E-F. Scale bar in I is 10 μm and applies to H-I. Error bars in all graphs
962 represent SD.

963

Movies

Movie 1. Border cell migration in control RNAi egg chambers. Lifeact-GFP and RNAi transgenes expressed under control of *slbo*-GAL4. 30 mins.

Movie 2. Border cell migration in *raskol* RNAi egg chambers.

Movie 3. Border cell delamination defects in *raskol* RNAi egg chambers.

Movie 4. Border cell cluster disassociation defects in *raskol* RNAi egg chambers.

Supplemental Figure Legends

S1 Fig. DE-Cad levels are not reduced in BCs expressing RNAi against target genes with low ERC values. A-D. Representative images of BC clusters expressing DE-Cad-GFP and UAS-RNAi constructs in the BCs under the control of *slbo*-GAL4. Expression of UAS-RFP (A) and *CG5875* RNAi (D) did not result in significantly difference in DE-Cad levels at the BC-BC contacts relative to control. B. Expression of *Hrb98DE* RNAi (B) reduced DE-Cad levels at BC-BC contacts relative to control. C. Expression of *capt* RNAi (C) increased levels of DE-Cad at BC contacts relative to control. PC boundaries are marked by dashed lines. E. Quantification of DE-Cad levels at the BC-BC contacts of UAS-RFP (n=75), *Hrb98DE* (n=72), *capt* (n=60) and *CG5875* (n=60) RNAi expressing clusters. *** - $p<0.001$, ** - $p<0.01$. Error bars represent mean ± SD. Scale bar in D is 10 μm and applies to A-D.

S2 Fig. Raskol colocalizes with DE-Cad in the FE. A. Dorsal view of the FE in egg chamber expressing Raskol-YFP and stained for DE-Cad (red) and F-actin (blue). Raskol is enriched at the apical surface of the FE and colocalizes with DE-Cad and F-actin. B. Cross-sectional images of the FE. Raskol colocalizes with DE-Cad and F-actin at the apical membrane of FE cells (arrows). Raskol also colocalizes with DE-Cad at PC contacts (arrowheads). In B, FE apical membrane faces the NCs. Individual channels correspond to the outlined box in the merged image. Scale bar in B is 10 μm and applies to A and B.

S3 Fig. Raskol colocalizes with DE-Cad in the amnioserosa and ectodermal cells during DC. A-D. Time-lapse images of Raskol-YFP and DE-Cad-RFP embryos during DC. Raskol colocalizes with DE-Cad at cell contacts in the amnioserosa (arrows).

994 Raskol colocalizes with DE-Cad at the zippering interface of dorsal most ectodermal
995 cells (arrowheads). Individual channels correspond to the outlined box in the merged
996 image. Scale bar in D is 10 μm and applies to all panels.

997 **S4 Fig. Coexpression pattern of *shg* and *raskol*.** A. Mean cytoplasmic levels of
998 Raskol in PCs and BCs relative to NCs. Cytoplasmic levels of Raskol are significantly
999 higher in PCs compared to BCs according to Welch's t-test (n=58, $p<0.0001$). B. *shg*
1000 and *raskol* expression patterns display similar trends during embryonic development.
1001 RNA-seq based expression data (obtained from www.flybase.org) in *Drosophila*
1002 embryos were plotted for *shg* and *raskol* during embryonic stages (2 hr increments).
1003 Expression of both *shg* and *raskol* peaks at 6-8 hr after egg laying.

1004

1005 **S1 Table. Top 500 shg ERC hits**

1006 **S2 Table. Enrichment analysis of shg ERC human orthologs: canonical pathways**

1007 **S3 Table. Enrichment analysis of shg ERC human orthologs: disease**

1008 **S4 Table. RNAi stocks used in this study**

1009 **S5 Table. Border cell migration and cluster disassociation data**

Figure 1

A

	armadillo	α-Catenin	shotgun
α-Catenin	-0.31		
shotgun	-0.31	0.47	
p120ctn	-0.26	0.60	0.26

B

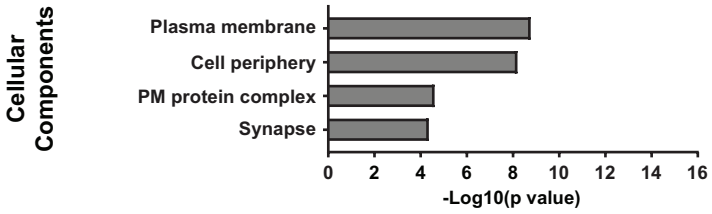

C

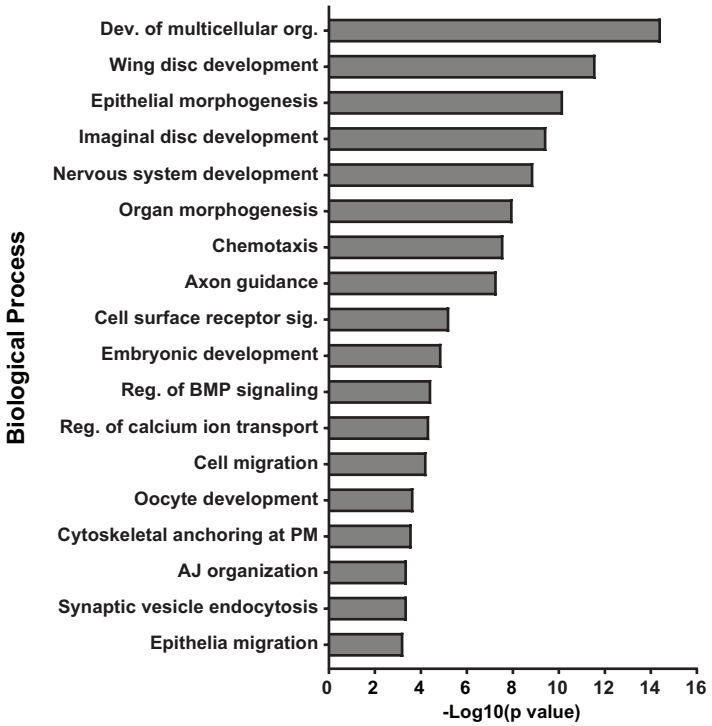

D

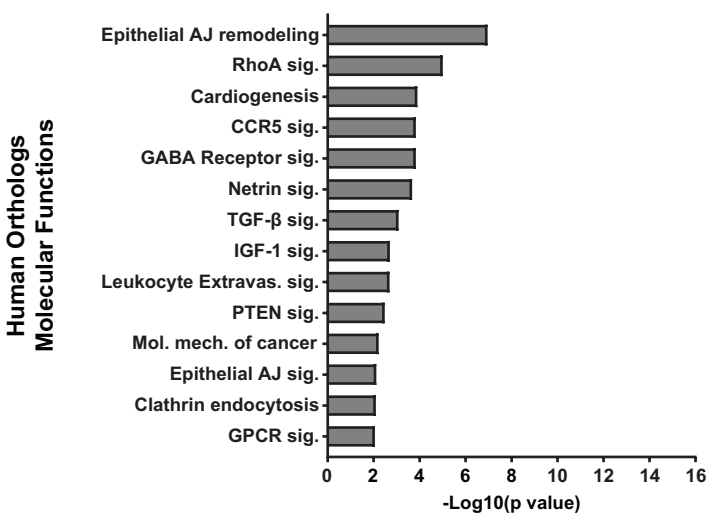

Figure 2

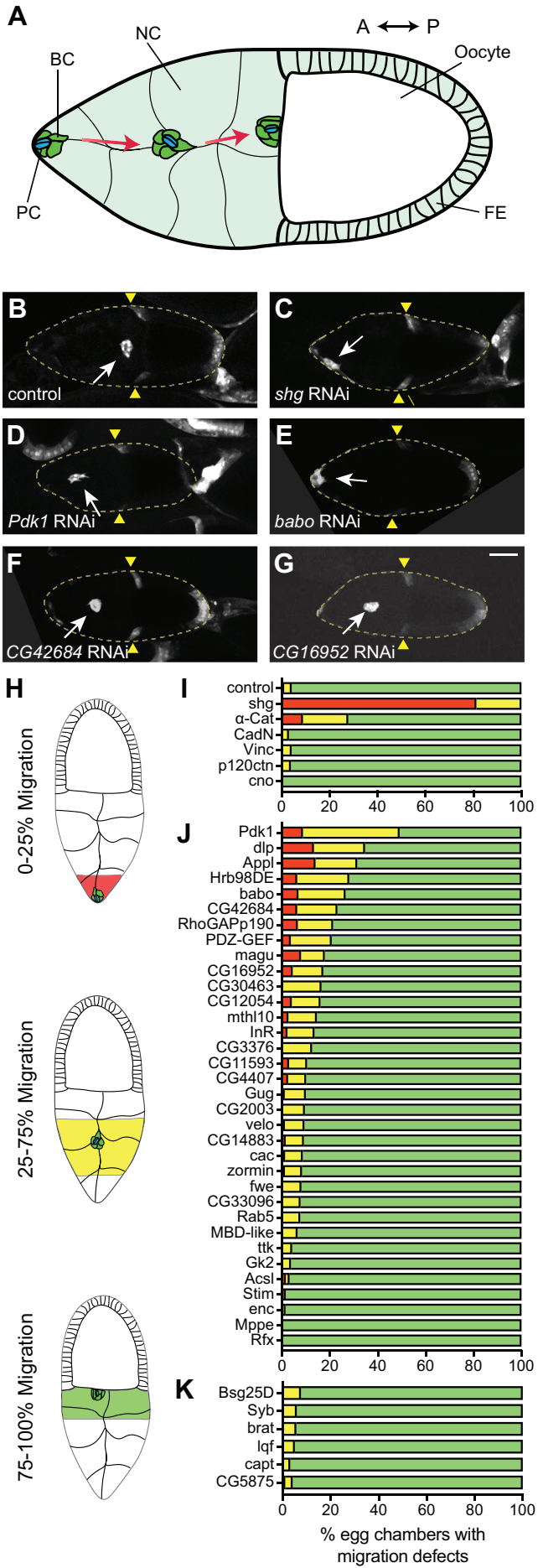

Figure 3

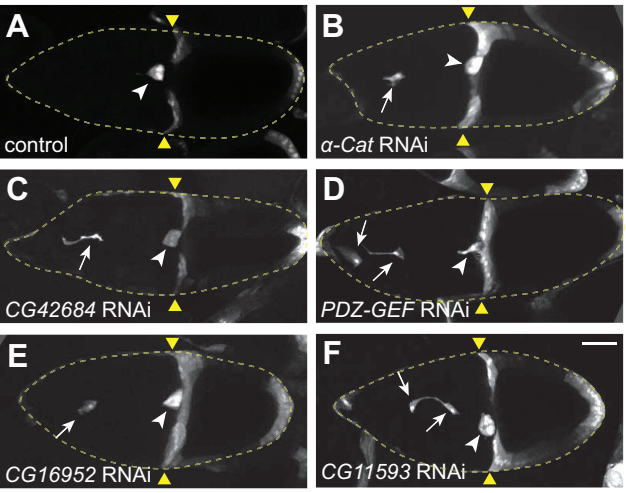

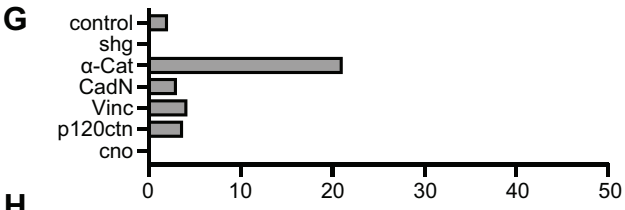

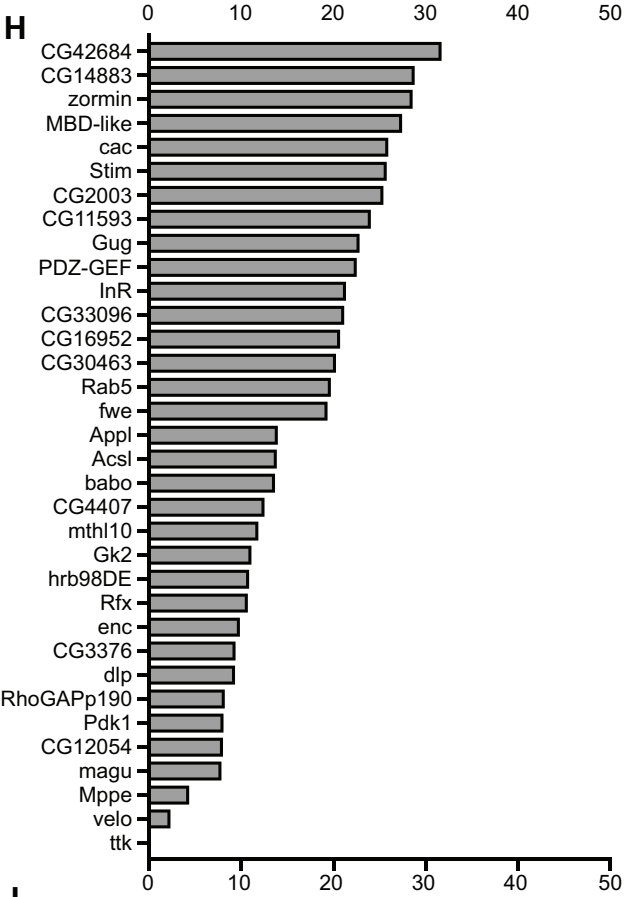

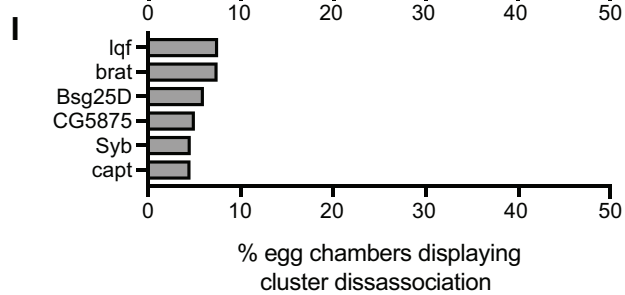

Figure 4

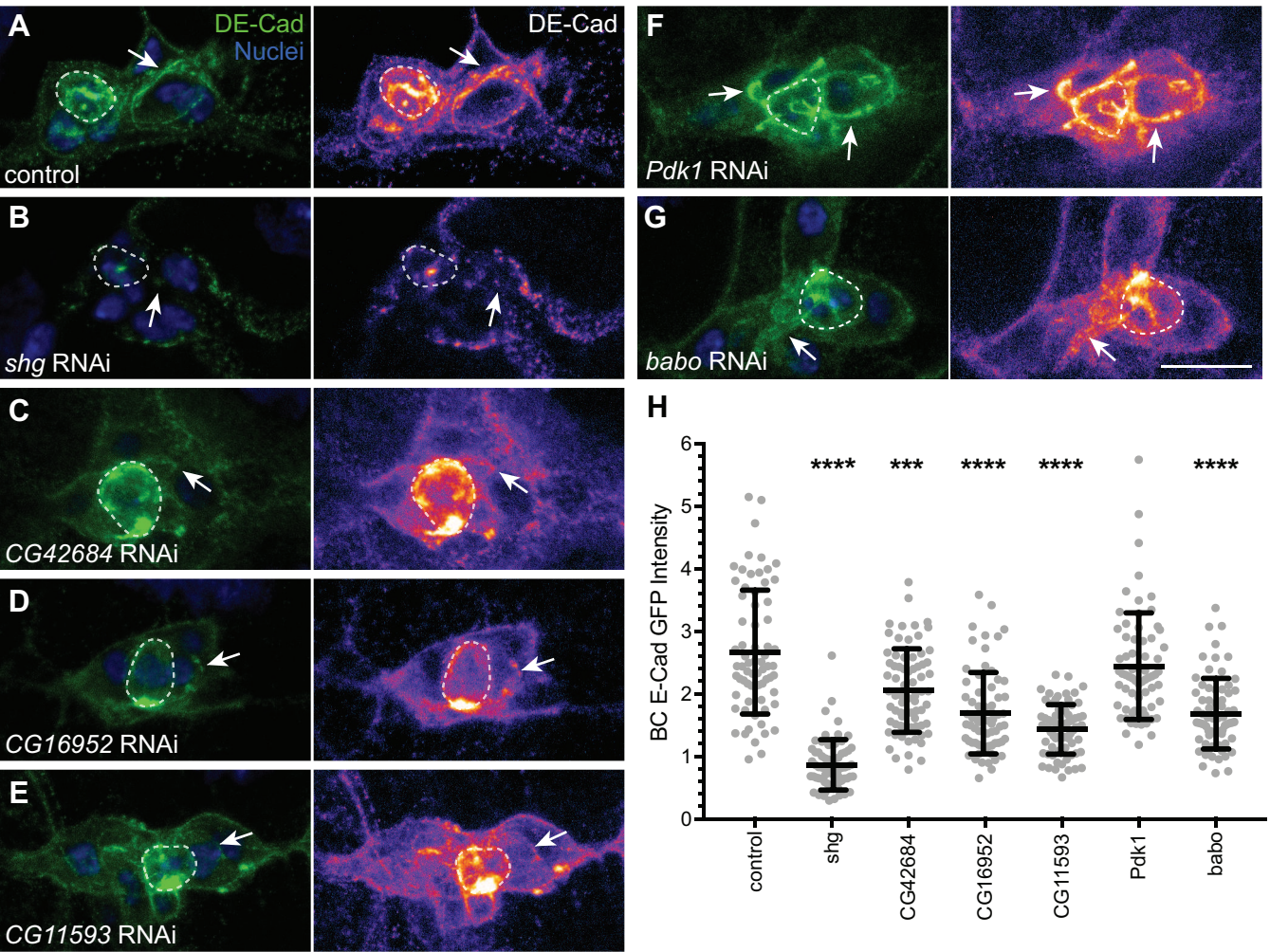

Figure 5

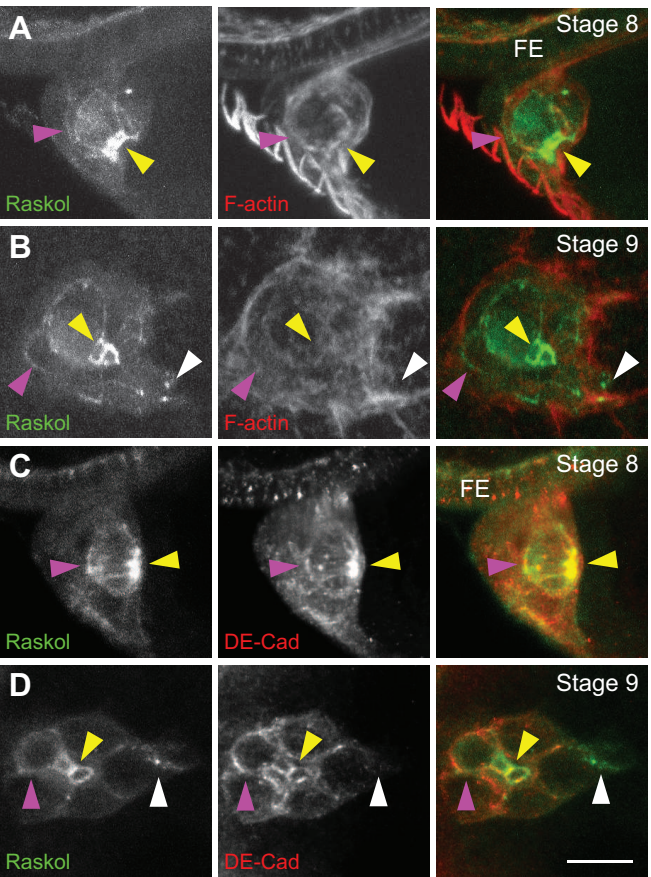

Figure 6